https://doi.org/10.15407/ujpe69.3.179

L.A. BULAVIN,[1] YE.G. RUDNIKOV,[1,2] S.O. SAMOILENKO[3]

[1] Taras Shevchenko National University of Kyiv,
Department of Molecular Physics, Faculty of Physics
(64, Volodymyrska Str., Kyiv 01601, Ukraine; e-mail: bulavin221@gmail.com)
[2] National Technical University of Ukraine "Igor Sikorsky Kyiv Polytechnic Institute",
Department of Biomedical Cybernetics, Faculty of Biomedical Engineering
(37, Beresteiskyi Ave., Kyiv 03056, Ukraine; e-mail: rudnikof@yahoo.com)
[3] Poltava State Medical University, Department of Physics
(23, Shevchenka Str., Poltava, 36011, Ukraine; e-mail: s.samoilenko@pdmu.edu.ua)

PHASE DIAGRAMS OF WATER ISOTOPOLOGUES AND NOBLE SUBSTANCES

Phase diagrams calculated using the literature data for water isotopologues and noble substances have been presented. The principle of corresponding states when caloric variables are applied was verified. It was shown that in the reduced temperature, pressure, and chemical potential coordinates, the water isotopologues form a group of substances and have similar phase diagrams. On the other hand, inert substances, starting from argon, form another group with similar phase diagrams in the same coordinates. At the same time, helium and neon, for which the de Boer quantum parameter is substantial, have phase diagrams different from those for other noble substances. Phase diagrams of tritiated water, T_2O, and radon, Rn, have been predicted.

K e y w o r d s: water isotopologues, superheavy water, noble substances, radon, chemical potential, phase diagrams, Kirchhoff equation, Massier functions, triple point.

1. Introduction

Nowadays, despite a considerable body of experimentally obtained thermodynamic data for most substances, the fundamental principle of corresponding states has not been thoroughly tested yet. In our opinion, such a procedure will allow not only the adequacy of the indicated fundamental statement to be verified but also the thermodynamic properties of some substances, which are still absent for various technical reasons, to be predicted.

According to Refs. [1–3], despite a substantial difference between the properties of water and argon, if the temperature T is low ($T \ll T_c$, where T_c is the corresponding critical temperature), there is an interval where the principle of corresponding states is applicable. In our previous works [4–6], the thermodynamic properties of one of the inert substances, namely, argon, were compared with those of water. The cited works confirmed the existence of a region of thermodynamic similarity between water and argon. At the same time, it was shown that there also exists a region of thermodynamic parameters where the properties of water and argon differ substantially.

C i t a t i o n: Bulavin L.A., Rudnikov Ye.G., Samoilenko S.O. Phase diagrams of water isotopologues and noble substances. *Ukr. J. Phys.* **69**, No. 3, 179 (2024). https://doi.org/10.15407/ujpe69.3.179.

Цитування: Булавін Л.А., Рудніков Є.Г., Самойленко С.О. Фазові діаграми ізотопологів води та інертних речовин. *Укр. фіз. журн.* **69**, №3, 179 (2024).

Liquid water can be considered as one of the most complicated liquids in nature due to a number of its anomalous properties [7–11]. In particular, water has unique parameters as a solvent [12–14].

The aim of this work is to compare, on the basis of the principle of corresponding states, the phase diagrams of H_2O, D_2O, and a number of inert substances (He, Ne, Ar, Kr, and Xe), which were obtained from available experimental data. For this purpose, the values of the chemical potential of the indicated substances were calculated as the functions of the temperature and pressure. When constructing the phase diagrams and to make their analysis more thorough, besides the thermodynamic potentials [15], the Massier (Massier-Planck) functions [16] were also used.

2. Chemical Potential Calculation Technique

To plot the phase diagrams of indicated substances in the temperature-pressure (T–P) coordinates, the most reliable literary experimental data were taken from articles, monographs, and reference books [17–19], as well as from physical databases [20–27].

In order to calculate the chemical potential along the vaporization, melting, and sublimation coexistence curves, a method to choose reference points for the entropy S and the internal energy E was proposed [5]. If following it, the entropy values are reckoned from the absolute zero temperature, and the internal energy from its value at the triple point. In contrast to many known variants of such a selection [18, 21–23], the method proposed by us to reckon S and E does not contradict the principle of corresponding states. According to the Gibbs phase rule [28, 29], a one-component liquid is a bivariant system, so its chemical potential μ is truly defined if its two independent variables are defined; for example, these can be the entropy and the internal energy of the system, $\mu = \mu(E, S)$.

The dimensionless ratio μ/μ_c between the chemical potential μ and its critical value μ_c is used. After the fixation of the reference points for reckoning S in kJ/(kg K) units and E in kJ/kg units, the chemical potential μ was calculated in kJ/kg units on the basis of the first principle of thermodynamics [15]

$$\mu = E - TS + PV. \tag{1}$$

Here $V = 1/\rho$ (in m^3/kg units) is the specific volume and ρ (in kg/m^3 units) is the mass density of the substance. Accordingly, the critical value of chemical potential was determined from formula (1) at the critical point [30, 31]. The phase diagrams presented below were plotted in dimensionless physical variables, i.e., normalized by their critical values.

In Table 1, literature data for the researched substances are quoted, as well as the molar and mass calibration parameters for the entropy and enthalpy [18,21–23,26,27], which were calculated using the proposed method of selecting their reference points. Note that at the temperature $T = 298$ K and the pressure $P = 1$ bar, inert substances are in the vapor state, whereas water isotopologues are in the liquid state. For water isotopologues, Table 1 also contains the indicated parameters for the vapor phase on the coexistence curve at the temperature $T = 298$ K [32, 33].

Table 1. **Calibration parameters – entropy (S^*, per mole, and S, per mass unit) and enthalpy (H^*, per mole, and H, per mass unit) – for the studied substances in the vapor (V) and liquid (L) phases**

Substance (phase)	S^*(298 K) kJ/mol-K	H^*(298 K), kJ/mol	S(298 K), kJ/kg-K	H(298 K), kJ/kg
H_2O (V)	217.485	45876.0	12.072	2546.5
H_2O (L)	69.95	1888.6	3.8828	104.922
D_2O (V)	228.770	47220.3	11.423	2357.8
D_2O (L)	76.390	1788.4	3.8143	89.382
T_2O (V)	235.413	48453.3	10.685	2199.3
T_2O (L)	78.52	1741.4	3.5640	79.041
Ne (V)	146.214	7500.6	7.2516	371.70
Ar (V)	154.732	11042.6	3.8763	276.42
Kr (V)	163.971	12936.3	1.9582	154.38
Xe (V)	169.573	15579.6	1.2925	118.66
Rn (V)	176.124	20159.5	0.7934	90.809

3. Comparison of Phase Diagrams of Water Isotopologues and Inert Substances

In Fig. 1, phase diagrams for water isotopologues and inert substances are plotted in the coordinates P/P_c vs T/T_c. As one can see, the phase diagrams of H_2O and D_2O are qualitatively similar to each other but substantially different from the phase diagrams of inert substances. The phase diagrams of inert substances, starting from argon, form another group of substances with similar behavior. An analysis of the phase diagrams of inert substances shows that neon

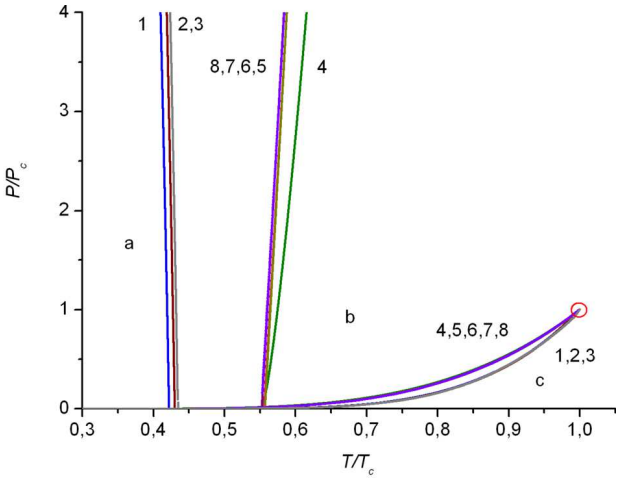

Fig. 1. Phase diagrams in the (P/P_c)-vs-(T/T_c) coordinates for water isotopologues [H_2O (*1*), D_2O (*2*), T_2O (*3*)] and inert substances [Ne (*4*), Ar (*5*), Kr (*6*), Xe (*7*), Rn (*8*)]; solid phase (*a*), liquid (*b*), vapor (*c*). The circle marks the critical point. The dependencies for T_2O and Rn are predicted

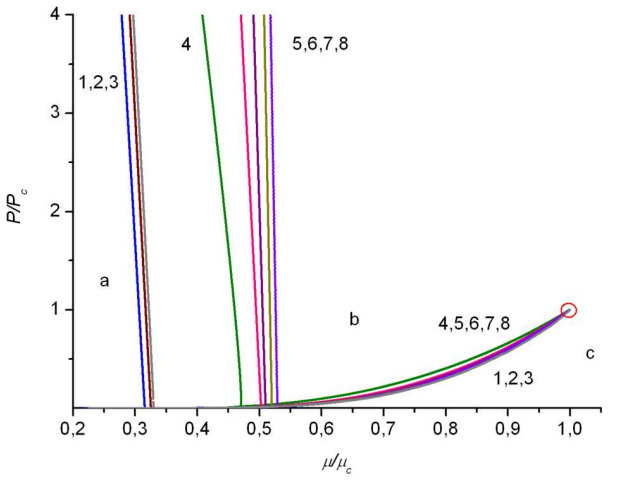

Fig. 2. Phase diagrams in the (P/P_c)-vs-(μ/μ_c) coordinates for water isotopologues [H_2O(*1*), D_2O (*2*), T_2O (*3*)] and inert substances [Ne (*4*), Ar (*5*), Kr (*6*), Xe (*7*), Rn (*8*)]; solid phase (*a*), liquid (*b*), vapor (*c*). The circle marks the critical point. The dependencies for T_2O and Rn are predicted

and, especially, helium, for which the role of the de Boer quantum parameter is significant, demonstrate phase diagrams that are different from those of other inert substances.

Unlike the case of inert substances, the inequality $(\partial P/\partial T)_u < 0$ takes place for H_2O and D_2O along the melting curve when departing from the triple points. After reaching the minimum temperature at which the thermodynamically balanced liquid state can exist (the triple point liquid-ice-ice at 251.165K for H_2O [34] and 254.35 K for D_2O [35]), the sign of this derivative changes as the pressure increases, $(\partial P/\partial T)_u > 0$.

At the same time, for inert substances, the inequality $(\partial P/\partial T)_u > 0$ holds within the whole temperature and pressure intervals.

In Fig. 2, phase diagrams for water isotopologues and inert substances are plotted in the coordinates P/P_c vs μ/μ_c. Again, similarly to the case of P/P_c-vs-T/T_c coordinates (Fig. 1), the phase diagrams of H_2O and D_2O (Fig. 2) form a separate group, which is different from the phase diagrams of inert substances. For water isotopologues, when moving away from the triple point along the melting curve, the inequality $(\partial P/\partial \mu)_u > 0$ $[(\mu_c/P_c)\ (\partial P/\partial \mu)_u < 0]$ takes place. The triple points of H_2O and D_2O correspond to the relative pressures P/P_c that are two orders of magnitude smaller than the corresponding values for

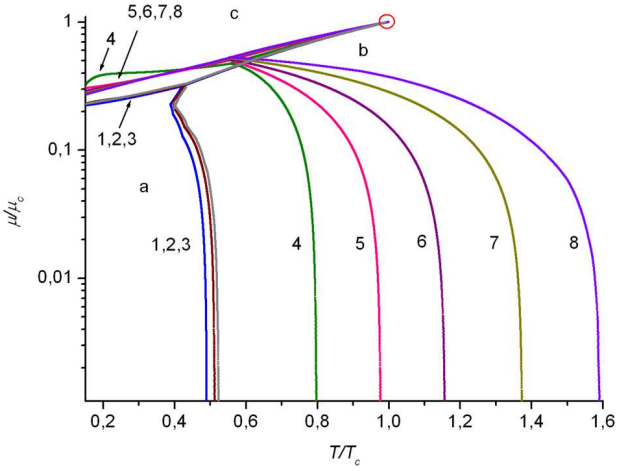

Fig. 3. Phase diagrams in the (μ/μ_c)-vs-(T/T_c) coordinates for water isotopologues [H_2 O(*1*), D_2O (*2*), T_2O (*3*)] and inert substances [Ne (*4*), Ar (*5*), Kr (*6*), Xe (*7*), Rn (*8*)]; solid phase (*a*), liquid (*b*), vapor (*c*). The circle marks the critical point. The dependencies for T_2O and Rn are predicted

inert substances. They also correspond to smaller relative values of the ratio μ/μ_c. In addition, the same inequality $(\partial P/\partial \mu)_u < 0$ $[(\mu_c/P_c)\ (\partial P/\partial \mu)_u > 0]$ takes place on the sublimation curve as occurred on the evaporation curve.

In Fig. 3, phase diagrams for H_2O, D_2O, and inert substances are plotted in the coordinates μ/μ_c vs T/T_c. Now again, as it was with the previous coor-

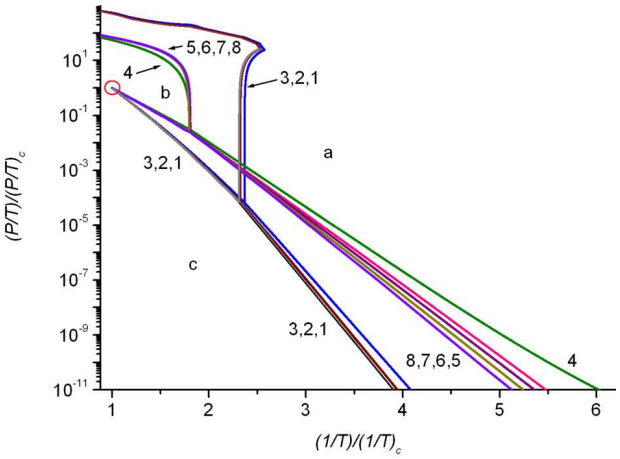

Fig. 4. Phase diagrams in the $(P/T)/(P_c/T_c)$-vs-$(1/T)/(1/T_c)$ coordinates for water isotopologues [H_2O (*1*), D_2O (*2*), T_2O (*3*)] and inert substances [Ne (*4*), Ar (*5*), Kr (*6*), Xe (*7*), Rn (*8*)]; solid phase (*a*), liquid (*b*), vapor (*c*). The circle marks the critical point. The dependencies for T_2O and Rn are predicted

dinate sets, the phase diagrams for H_2O and D_2O (Fig. 3) form a separate group, and they differ from the phase diagrams of inert substances. For H_2O and D_2O, in contrast to inert substances, the inequality $(\partial\mu/\partial T)_u < 0$ $[(T_c/\mu_c)\,(\partial\mu/\partial T)_u > 0]$ holds when moving away from the triple point along the melting curve. As the ratio μ/μ_c decreases and the temperature reaches a minimum at which a thermodynamically balanced liquid state for liquid-ice-ice triple point can exist, the sign of this derivative changes, $(\partial\mu/\partial T)_u > 0$ $[(T_c/\mu_c)\,(\partial\mu/\partial T)_u < 0]$. For the inert substances, the inequality $(\partial\mu/\partial T)_u > 0$ $[T_c/\mu_c\,(\partial\mu/\partial T)_u < 0]$ takes place along the curve melting within the whole interval of the parameters T/T_c and μ/μ_c. For the sublimation and evaporation curves of all considered substances, the inequality $(\partial\mu/\partial T)_u < 0$ $[(T_c/\mu_c)\,(\partial\mu/\partial T)_u > 0]$ takes place. As one can see, the analyzed phase diagrams confirm the adequacy of the principle of corresponding states separately for two groups of substances, water isotopologues and inert substances starting from argon.

When plotting the phase diagrams, in order to analyze them in more detail, besides conventional thermodynamic potentials, the Massier (Massier–Planck) functions [16] were also involved. Historically, the group of Massier functions was proposed earlier than the thermodynamic potentials. They have a mathematical structure identical to that of thermodynamic potentials. The Massier functions have the entropy dimensionality. They are related to each other and to the thermodynamic potentials by the Legendre transformations. Those functions arise when the quantities μ/T (the Planck potential) and $-P/T$ (the Kramers potential) are written as the total differentials of the corresponding characteristic functions:

$$d(\mu/T)(P/T, 1/T) \text{ and } d(P/T)(\mu/T, 1/T).$$

To obtain the differentials of the indicated variables, let us rewrite the Gibbs–Duhem equation [15] in two other possible notation forms,

$$d(\mu/T) = V \cdot d(P/T) + E \cdot d(1/T) \tag{2}$$

and

$$d(P/T) = (1/V)\,d(\mu/T) - (E/V)\,d(1/T) =$$

$$= \rho\,d(\mu/T) - \varepsilon\,d(1/T). \tag{3}$$

Formulas (2) and (3) describe relationships between the new variables $1/T$, P/T, and μ/T. Like the variables T, P, and μ, which are more commonly used today, they are also continuous at the phase transition of the first kind. In expression (3), the notation ε (in kJ/m^3 units) is used for the internal energy per unit volume.

The phase diagrams of water isotopologues and inert substances in the reduced coordinates $(P/T)/(P_c/T_c)$ vs $(1/T)/(1/T_c)$ are depicted in Fig. 4. One can see that in contrast to the group of inert substances, the inequality $(\partial(P/T)/\partial(1/T))_u > 0$ takes place for H_2O and D_2O when departing from the triple point along the melting curve. As the pressure increases and the temperature reaches a minimum at which the thermodynamically equilibrium liquid state can exist at the liquid-ice-ice triple point, the sign of the derivative changes, $(\partial(P/T)/\partial(1/T))_u < 0$. For inert substances, the inequality $(\partial(P/T)/\partial(1/T))_u < 0$ holds within the whole intervals of temperature and pressure.

An analysis of Fig. 4 shows that, unlike Fig. 1, the sublimation curves and the low-temperature sections of the evaporation curves for light water, heavy water, and inert substances (except for neon and helium [36–39]) are straight lines in accordance with the Kirchhoff formula, which has a molecular-kinetic

substantiation [40, 41],

$$\ln\ P = A - \frac{B}{T} - C \ln\ T. \tag{4}$$

Here A, B, and C are constants. At low temperatures, according to (4), $\ln\ P \sim 1/T$. Helium and neon, for which the role of the so-called de Bohr quantum parameter is substantial, deviate from the Kirchhoff equation. In Table 2, the values of the de Boer parameter for the inert substances are quoted.

The phase diagrams of light water, heavy water, and inert substances in the coordinates $(P/T)/(P_c/T_c)$ vs $(\mu/T)/(\mu_c/T_c)$ are shown in Fig. 5. As one can see, the influence of the de Boer quantum parameter becomes appreciable starting from neon (Table 2). For all phase diagrams depicted in Fig. 5, the inequality $(\partial(P/T)/\partial(\mu/T))_u > 0$ $[(\mu_c/P_c) \cdot (\partial(P/T)/\partial(\mu/T))_u < 0]$ takes place when departing from the triple point along the melting curve. At the same time, the values of the relative quantity $(P/T)/(P_c/T_c)$ for H_2O and D_2O at their triple points are two orders of magnitude less than their counterparts for the inert substances. The inequality $(\partial(P/T)/\partial(\mu/T))_u > 0$ $[(\mu_c/P_c) \cdot (\partial(P/T)/\partial(\mu/T))_u < 0]$ holds on the sublimation curve, but the inverse inequality $(\partial(P/T)/\partial(\mu/T))_u < 0$ $[(\mu_c/P_c) \cdot (\partial(P/T)/\partial(\mu/T))_u > 0]$ holds on the evaporation curve. So, unlike the phase diagrams in the coordinates P/P_c vs μ/μ_c (see Fig. 2), the same inequality as on the melting curve is obeyed on the sublimation curve in the coordinates $(P/T)/(P_c/T_c)$ vs $(\mu/T)/(\mu_c/T_c)$ (see Fig. 5).

The phase diagrams of H_2O, D_2O, and inert substances in the reduced coordinates $(\mu/T)/(\mu_c/T_c)$ vs $(1/T)/(1/T_c)$ are plotted in Fig. 6. A corresponding analysis shows that for H_2O and D_2O, the triple point corresponds to smaller values of the dimensionless parameter $(\mu/T)/(\mu_c/T_c)$ than for the group of inert substances. Unlike inert substances, for H_2O and D_2O, when departing from the triple point along the melting curve, the inequality $(\partial(\mu/T)/\partial(1/T))_u > 0$ $[(1/\mu_c)(\partial(\mu/T)/\partial(1/T))_u < 0]$ holds. As the value of $(\mu/T)/(\mu_c/T_c)$ decreases and the temperature reaches a minimum value at which the thermodynamically balanced liquid state at the liquid–ice–ice triple point can exist, the sign of this derivative changes, $(\partial(\mu/T)/\partial(1/T))_u < 0$ $[(1/\mu_c)(\partial(\mu/T)/\partial(1/T))_u > 0)]$. For the inert substances, the inequality $(\partial(\mu/T)/\partial(1/T))_u < 0$ $[(1/\mu_c)(\partial(\mu/T)/\partial(1/T))_u > 0]$

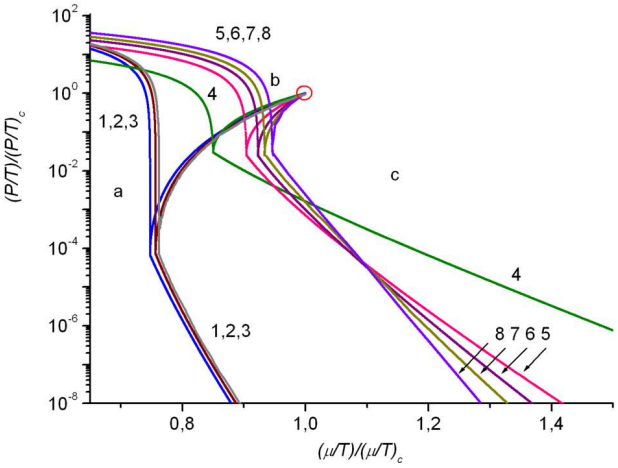

Fig. 5. Phase diagrams in the $(P/T)/(P_c/T_c)$-vs-$(\mu/T)/(\mu_c/T_c)$ coordinates for water isotopologues [H_2O (*1*), D_2O (*2*), T_2O (*3*)] and inert substances [Ne (*4*), Ar (*5*), Kr (*6*), Xe (*7*), Rn (*8*)]; solid phase (*a*), liquid (*b*), vapor (*c*). The circle marks the critical point. The dependencies for T_2O and Rn are predicted

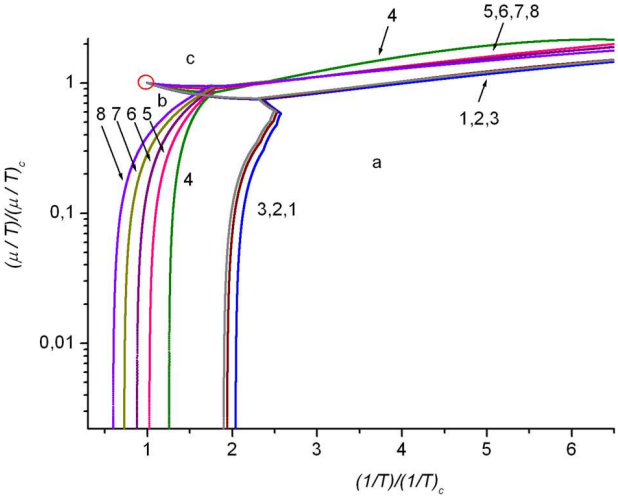

Fig. 6. Phase diagrams in the $(\mu/T)/(\mu_c/T_c)$-vs-$(1/T)/(1/T_c)$ coordinates for water isotopologues [H_2O (*1*), D_2O (*2*), T_2O (*3*)] and inert substances [Ne (*4*), Ar (*5*), Kr (*6*), Xe (*7*), Rn (*8*)]; solid phase (*a*), liquid (*b*), vapor (*c*). The circle marks the critical point. The dependencies for T_2O and Rn are predicted

Table 2. **De Boer parameter $\Lambda = h/(\sigma\sqrt{Mu})$ for inert substances [37, 42]**

Substance	^{3}He	^{4}He	Ne	Ar	Kr	Xe	Rn
Λ	3.1	2.7	0.59	0.19	0.10	0.064	0.047

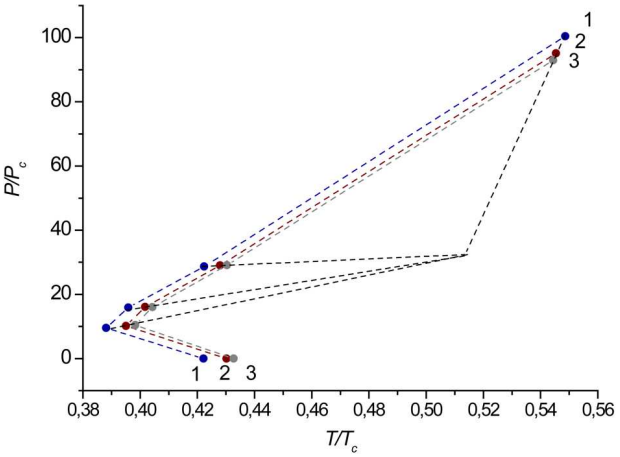

Fig. 7. Relative arrangement of triple points of water isotopologues in the plane reduced pressure vs reduced temperature (P/P_c vs T/T_c): H_2O (*1*), D_2O (*2*), T_2O (*3*). Triple points for T_2O at high pressure are predicted

is satisfied along the melting curve within the whole intervals of change of the quantities $(\mu/T)/(\mu_c/T_c)$ and $(1/T)/(1/T_c)$.

The inequality $(\partial(\mu/T)/\partial(1/T))_u < 0$ $[(1/\mu_c) \times \times (\partial(\mu/T)/\partial(1/T))_u > 0]$ on the sublimation curves and the opposite inequality $(\partial(\mu/T)/\partial(1/T))_u > 0$ $[(1/\mu_c)\ (\partial(\mu/T)/\partial(1/T))_u < 0]$ on the evaporation curves take place for all considered substances. Unlike the phase diagrams shown in Fig. 3, the signs of the indicated inequalities are different on the sublimation and evaporation curves.

Thus, the phase diagrams plotted in the reduced coordinates and determined by the Massier functions (see Figs. 4 to 6) confirm that the water isotopologues form a single group of substances with similar behavior, whereas the inert substances form another group with similar behavior, but with some deviations in the case of helium and neon.

4. Prediction of Phase Diagrams for T_2O and Rn

The thermodynamic similarity of phase diagrams for light and heavy water makes it possible to predict the view of the phase diagrams for superheavy water. For this purpose, the critical parameters of superheavy water, T_2O, were taken from [43, 44]. In the cited works, by comparing the temperature dependences of the pressure, $P(T)$, for H_2O and D_2O along the vaporization curves, the critical parameters for superheavy water were predicted. Further analysis showed that the forecast of the dependences $P(T)$ for T_2O along the vaporization curve is one of the most reliable among other physical dependences. The phase diagrams predicted for superheavy water are exhibited in Figs 1 to 6.

Figure 7 demonstrates the relative arrangement of the parameters of the triple points of water isotopologues. In this phase diagram, the positions of the H_2O triple points at the liquid phase boundary were taken from Refs. [19, 34, 45, 46], their counterparts for D_2O were taken from Refs. [19, 35], and the position of the triple point liquid-vapor-solid in T_2O was taken from Refs. [43, 44] (see Table 3).

According to data [9, 34, 35, 45, 46], the inequality $(T_{\text{fus}}/T_c)(H_2O) < (T_{\text{fus}}/T_c)(D_2O)$ is obeyed for the triple points with the temperatures $T_{\text{fus}}/T_c < < 0.5$, and the inverse inequality $(T_{\text{fus}}/T_c)(H_2O) > > (T_{\text{fus}}/T_c)(D_2O)$ holds for the region $T_{\text{fus}}/T_c > 0.5$. According to Refs. [34,35], the melting curves for H_2O and D_2O in the P/P_c vs T/T_c coordinates are thermodynamically similar (see Fig. 7), and according to Refs. [43, 44, 47], the evaporation curves for H_2O, D_2O, and T_2O in the $P - T$ coordinates (and therefore in the $P/P_c - T/T_c$ coordinates) are also thermodynamically similar. Based on those results, we predicted the coordinates of the liquid-ice-ice triple points for T_2O at high pressures (see Fig. 7 and Table 3).

Note that, compared to light water H_2O, heavy water D_2O has a lower temperature of the triple point liquid–ice VI–ice VII (see Fig. 7 and Table 3), as well as its critical temperature (see Table 4), indicates weaker D-bonds compared to H-bonds [19, 60], while the trend changes to the opposite as the temperature decreases (see Fig. 7, Tables 3, 5).

We may assume [33,48–50] that the phase diagrams for a number of other water isotopologues are thermodynamically similar to the phase diagrams shown in Figs. 1 to 8 for H_2O, D_2O, and T_2O.

Following an analogous technique, the phase diagram similarity of the inert substances Ar, Kr, and Xe made it possible to suggest the view of the phase diagram for the inert substance radon, Rn (see Figs 1 to 6). The critical parameters of radon were taken from Ref. [17].

The values of the critical parameters and the triple-point parameters for the researched substances are quoted in Tables 4 and 5, respectively. Note that the presented values of caloric variables for H_2O, D_2O,

Table 3. **Values of the reduced parameters T_{fus}/T_c and P_{fus}/P_c at the triples points of water isotopologues [19, 34, 35, 45, 46]. The parameters for T_2O at high pressures are predicted**

Parameter	Substance					
	H_2O		D_2O		T_2O	
	T_{fus}/T_c	P_{fus}/P_c	T_{fus}/T_c	P_{fus}/P_c	T_{fus}/T_c	P_{fus}/P_c
Liquid–vapor–ice Ih	0.4221295	2.77216×10^{-5}	0.4301778	3.05438×10^{-5}	0.4326902	3.09745×10^{-5}
Liquid–ice Ih–ice III	0.3881394	9.5132342	0.3950454	10.1560336	0.3983	10.44
Liquid–ice III–ice V	0.3958646	15.8674764	0.401724	16.0649986	0.4043	16.02
Liquid–ice V–ice VI	0.4223613	28.662074	0.4279724	29.0370234	0.4304	29.10
Liquid–ice VI–ice VII	0.5486015	100.435098	0.545391	95.0974056	0.5444	92.95

Table 4. **Critical thermodynamic parameters of water isotopologues and noble substances**

Substance	M_r	T_c, K	P_c, MPa	μ_c^*, kJ/mol	ρ_c^*, kg/mol	S_c^*, kJ/mol-K	E_c^*, kJ/mol
H_2O	18.015	647.1	22.064	–54809.9	17.87373	142.73	36314
D_2O	20.027	643.89	21.671	–59676.2	17.77555	153.67	38041.7
T_2O	22.032	641.66	21.385	–64662.5	17.70193	164.69	39805.9
Ne	20.18	44.4	2.662	–1461.1	23.88058	62.043	1187.17
Ar	39.95	150.69	4.863	–8869.7	13.40743	89.919	4317.58
Kr	83.8	209.48	5.525	–15479.5	10.84976	105.24	6055.47
Xe	131.29	289.73	5.842	–24781.4	8.400488	116.95	8408.49
Rn	222.0	377.0	6.28	–35942.4	7.142793	126.8	10982.01

Ne, Ar, Kr, and Xe are calculated, whereas for T_2O and Rn they are predicted.

5. General Analysis of the Phase Diagrams of Examined Substances

As was indicated in Ref. [51], for the first-kind phase transition liquid-hexagonal ice in water at temperatures $\theta < 4°C$ and pressures $P < 28.33$ MPa, the coefficient of volume expansion

$$\alpha_P = \frac{1}{V}\left(\frac{\partial V}{\partial T}\right)_P = -\left(\frac{\partial \ln \rho}{\partial T}\right)_P = \frac{\langle \Delta S \Delta V \rangle}{k_{\mathrm{B}} T V} \qquad (5)$$

is negative, which means the anti-correlation between the entropy and volume fluctuations [51]. For heavy water, the coefficient of volume expansion (5) is negative at temperatures $\theta < 11$ °C below the line $\theta = \theta_{\max}(P, \rho_{\max})$ of maxima density $\rho = \rho_{\max}$.

According to our estimate obtained on the basis of experimental data [52], this line of maxima corresponds to pressures $P < 53.7$ MPa. For superheavy water, according to our prediction based on the principle of thermodynamic similarity, $\alpha_P < 0$ is fulfilled under the condition of $P < 65.3$ MPa. Since for

Table 5. **Thermodynamic parameters at the liquid-vapor-solid triple point of water isotopologues and noble substances**

Substance (phase)	T_{fus}, K	P_{fus}, kPa	μ^*_{fus}, kJ/kmol	ρ^*_{fus}, kmol/m^3	S^*_{fus}, kJ/kmol-K
H_2O (V)	273.16	0.61166	–17300.5	0.0002695	228.274
H_2O (L)				55.4970	63.3348
D_2O (V)	276.969	0.65989	–19434.3	0.0002874	238.090
D_2O (L)				55.1884	70.1702
T_2O (V)	277.64	0.66239	–21048.6	0.0003055	247.555
T_2O (L)				54.8855	77.0950
Ne (V)	24.55	43.355	–685.1	0.21870	101.0594
Ne (L)				61.9276	28.109
Ar (V)	83.806	68.891	–4459.8	0.10150	131.2692
Ar (L)				35.4653	55.6436
Kr (V)	115.78	73.5336	–7896.5	0.07845	146.6670
Kr (L)				29.1962	111.689
Xe (V)	161.36	81.7723	–12891.4	0.06263	158.3069
Xe (L)				22.5926	106.860
Rn (V)	202.16	93.06	–18332.8	0.04029	176.6454
Rn (L)				12.38	90.687

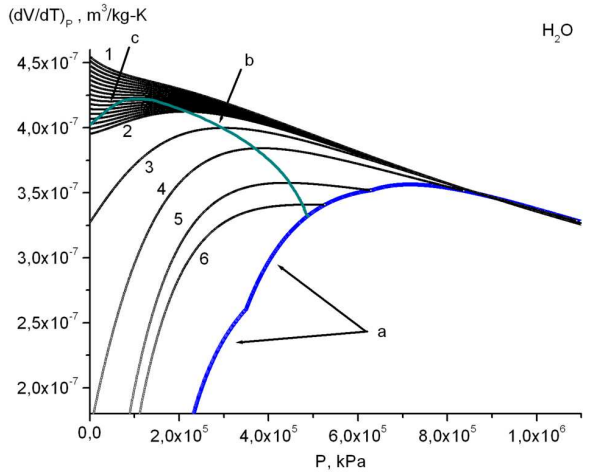

Fig. 8. Baric dependences of the derivative $(\partial V/\partial T)_P$ along the isotherms for water: the liquid-solid coexistence curve (a), the line of maxima of the derivative $(\partial V/\partial T)_P$ $[(\partial^2 V/\partial T\partial P) = 0$ and $(\partial^3 V/\partial T\partial P^2) < 0]$ (b), the line of minima of the derivative $(\partial V/\partial T)_P$ $[(\partial^2 V/\partial T\partial P) = 0$ and $(\partial^3 V/\partial T\partial P^2) > 0]$ (c); $T = 322$ (*1*), 314 (*2*), 306 (*3*), 290 (*4*), 273 (*5*), and 268 K (*6*)

H_2O $\log P < 1.45$, for D_2O $\log P < 1.73$ and for T_2O $\log P < 1.82$, and the pressure along the melting curve of these substances changes by more than seven orders of magnitude (see Fig. 1), these conditions can be considered quite close.

The reduction of volume fluctuations for H_2O and D_2O in the indicated intervals of temperature and pressure is a result of the growth of entropy fluctuations. According to the two-structure model of water in the liquid state [53–58], this means that if the temperature drops below 4 °C, the equilibrium of the dynamic phase transition between two structures (the LDW and HDW phases [57, 58]) shifts toward the more expanded structure, which is more ordered. The system entropy decreases at that, $(\partial S/\partial V)_P < 0$, whereas the specific volume of the system accordingly increases [51].

From the thermodynamic viewpoint, this occurs via the so-called thermodynamic compensation process: the reduction of the specific volume V due to the lowering of the kinetic energy of molecules, $\sim k_B T$, is compensated by the dominating process of volume growth due to the dynamic reconstruction of the water structure. In this case, the thermodynamic work has the opposite sign and is written as $-PdV$ instead of PdV, and the pressure $P(V)$ changes together with the change of the specific volume V [59].

In our recent works [4–6], we have analyzed the thermodynamic anomalies of water in the vicinity of its special temperature $\theta = 42$ °C [60–63]. In particular, in work [6]. It was shown that the anomalous behavior of the volume expansion coefficient α_P and the thermodynamic coefficient $(\partial V/\partial T)_P = \alpha_P V$ below the special water temperature of 42 °C appears due to the entropy contribution to those quantities. This conclusion agrees with the assumption that the local order in water changes below the indicated temperature. In particular, the lifetime of a local network of hydrogen bonds becomes long enough for a tetrahedral network characteristic of water and formed by tetrahedral structures of low density (the LWD phase [57, 58]) to gradually develop [64].

In work [4], it was also shown that the minimum of the derivative $-(\partial V/\partial P)_T$ along the liquid-vapor coexistence curve at a temperature of 42 °C is associated with the line of maxima $(\partial V/\partial T)_P = \alpha_P V$ in the pressure-temperature plane. In turn, the line of maxima $(\partial V/\partial T)_P$ arises owing to the anomalous nonmonotonic character of the variation in the quantity $(\partial V/\partial T)_P$ along the liquid-solid coexistence curve [65]. A more complete phase diagram $(\partial V/\partial T)_P$ than in the previous work [4] is presented in Fig. 8.

For heavy water, D_2O, and superheavy water, T_2O, the phase diagrams of the derivative $(\partial V/\partial T)_P$ (see Fig. 8) have similar forms and are shifted along the temperature axis toward higher values by $\Delta\theta \approx$ ≈ 3.5 °C and 5.5 °C, respectively.

From the phase diagram shown in Fig. 8, it follows that the specific temperature of water $\theta =$ $= 42$ °C is the endpoint of the line of minima of the derivative $(\partial V/\partial T)_P$, into which the line of maxima of this quantity is transformed in the pressure-temperature plane. On the other hand, the line of maxima of the derivative $(\partial V/\partial T)_P$ terminates at the liquid-solid coexistence curve at pressures for which the characteristic of water anomalous condition $(\partial P/\partial T)_u < 0$ (see Fig. 1), $(\partial \mu/\partial T)_u > 0$ (see Fig. 3), $(\partial(P/T)/\partial(1/T))_u > 0$ (see Fig. 4) and $(\partial(\mu/T)/\partial(1/T))_u > 0$ (see Fig. 6) are obeyed. Here the subscript u denotes the curve corresponding to the phase transition of the first kind.

Thus, the anomalous liquid-solid phase transition in water $(\partial P/\partial T)_u < 0$ is a combined effect of the anomalous peculiarities of water [4–6] both along the liquid-vapor coexistence curve $(\partial P/\partial T)_u > 0$ in the vicinity of its specific temperature $\theta = 42$ °C

and in the temperature-pressure plane below this temperature.

According to the two-structure model of water [53–58], if the temperature θ decreases, the reduction of the specific volume V, which occurs due to the decrease in the kinetic energy of molecules, $\sim k_{\rm B}T$, competes with the reduction of the entropy of liquid S [51]: the decrease of the entropy S of water and its isotopologues together with the lowering of the temperature θ occurs as a result of the growing role of a more expanded and more ordered structure, which counteracts the reduction of the specific volume. At temperatures $\theta < \theta_{\max}$, below the line of maxima $\theta_{\max} = \theta_{\max}(P, \rho_{\max})$ of the density $\rho = \rho_{\max}$ (where $\theta_{\max} \leq 3.984$ °C for H_2O, $\theta_{\max} \leq 11.185$ °C for D_2O, and $\theta_{\max} \leq 13.403$ °C for T_2O [18, 20, 66–69]), the role of the more expanded and more ordered structure becomes decisive [$(\partial P/\partial T)_u < 0$ and $(\partial V/\partial T)_P < 0$) [65]].

6. Conclusions

A comparison of the phase diagrams of water isotopologues and inert substances allows the following conclusions to be drawn.

1. The analyzed phase diagrams confirm the adequacy of the principle of corresponding states: the water isotopologues form a group of substances with a similar behavior. In turn, the inert substances, except for helium and neon, form another group of substances with similar behavior.

2. The similarity of the phase diagrams of light and heavy water made it possible to propose the phase diagram for superheavy water, T_2O, and the similarity of the phase diagrams for the inert substances Ar, Kr, and Xe made it possible to predict the phase diagram for radon, Rn.

3. Reference points for reckoning the entropy and the internal energy were proposed, which made it possible to verify the principle of corresponding states in caloric variables.

4. It was shown that the anomalous phase transition of the first kind liquid-hexagonal ice in water arises due to the existence of the specific water temperature $\theta = 42$ °C, at which the thermodynamic coefficient $-(\partial V/\partial P)_T$ reaches its minimum value, which can be explained in the framework of the two-structure model of water (the LDW and HDW phases).

1. A.I. Fisenko, N.P. Malomuzh, A.V. Oleynik. To what extent are thermodynamic properties of water argon-like? *Chem. Phys. Lett.* **450**, 297 (2008).
2. I.V. Zhyganiuk, M.P. Malomuzh. Physical nature of hydrogen bond. *Ukr. J. Phys.* **60**, 960 (2015).
3. L.A. Bulavin, V.Ya. Gotsulskyi, N.P. Malomuzh, A.I. Fisenko. Crucial role of water in the formation of basic properties of living matter. *Ukr. J. Phys.* **65**, 794 (2020).
4. L.A. Bulavin, Ye.G. Rudnikov. Temperature and pressure effect on the thermodynamics coefficient $(dV/dT)P$ of water. *Ukr. J. Phys.* **68**, 122 (2023).
5. L.A. Bulavin, Ye. G.Rudnikov. The influence of the temperature and chemical potential on the thermodynamic coefficient $-(dV/dP)T$ of water. *Ukr. J. Phys.* **68**, 390 (2023).
6. L.A. Bulavin, Ye.G. Rudnikov, A.V. Chalyi. Thermodynamic anomalies of water near its singular temperature of 42 °C. *J. Mol. Liq.* **389**, 122849 (2023).
7. G.M. Kontogeorgis, A. Holster, N. Kottaki, E. Tsochantaris, F. Topsøe, J. Poulsen, M. Bache, X. Liang, N.S. Blom, J. Kronholm. Water structure, properties and some applications. A review. *Chem. Thermodyn. Thermal Anal.* **6**, 100053 (2022).
8. H. Tanaka. Roles of liquid structural ordering in glass transition, crystallization, and water's anomalies. *J. Non-Cryst. Solids X* **13**, 100076 (2022).
9. M.F. Chaplin. Structure and properties of water in its various states. In: *Encyclopedia of Water: Science, Technology, and Society.* Edited by P.A. Maurice (Wiley, 2019).
10. V. Pogorelov, I. Doroshenko, G. Pitsevich, V. Balevicius, V. Sablinskas, B. Krivenko, L.G.M. Pettersson. From clusters to condensed phase – FT IR studies of water. *J. Mol. Liq.* **235**, 7 (2017).
11. G. Pitsevich, I. Doroshenko, A. Malevich, E. Shalamberidze, V. Sapeshko, V. Pogorelov, L.G.M. Pettersson. Temperature dependence of the intensity of the vibration-rotational absorption band ν_2 of H_2O trapped in an argon matrix. *Spectrochim. Acta A* **172**, 83 (2017).
12. O.V. Tomchuk, L.A. Bulavin, V.L. Aksenov, V.M. Garamus, O.I. Ivankov, A.Y. Vul', A.T. Dideikin, M.V. Avdeev. Small-angle scattering from polydisperse particles with a diffusive surface. *J. Appl. Crystallogr.* **47**, 642 (2014).
13. E.A. Kyzyma, A.A. Tomchuk, L.A. Bulavin, V.I. Petrenko, L. Almasy, M.V. Korobov, D.S. Volkov, I.V. Mikheev, I.V. Koshlan, N.A. Koshlan, P. Bláha, M.V. Avdeev, V.L. Aksenov. Structure and toxicity of aqueous fullerene C_{60} solutions. *J. Surf. Investig. X-ray Synchr. Neutr. Techn.* **9**, 1 (2015).
14. V.I. Petrenko, O.P. Artykulnyi, L.A. Bulavin, L. Almásy, V.M. Garamus, O.I. Ivankov, N.A. Grigoryeva, L. Vekas, P. Kopcansky, M.V. Avdeev. On the impact of surfactant type on the structure of aqueous ferrofluids. *Colloid. Surface. A* **541**, 222 (2018).
15. J.H.S. Lee, K. Ramamurthi. *Fundamentals of Thermodynamics* (CRC Press, 2022).

16. V.V. Sychev. *The Differential Equations Of Thermodynamics* (CRC Press, 1991).
17. C. Yaws. *Thermophysical Properties of Chemicals and Hydrocarbons*. 2nd edition (Gulf Professional Publishing, 2014).
18. M.Z. Southard, D.W. Green. *Perry's Chemical Engineers' Handbook* (Mcgraw-Hill Education, 2019).
19. M.F. Chaplin. Water Structure and Science; https:// water.lsbu.ac.uk/water/water_structure_science.html.
20. *Thermophysical Properties of Fluid Systems. NIST Chemistry WebBook, SRD 69*; https://webbook.nist.gov/ chemistry/fluid.
21. *MiniRefprop Database, NIST;* https://trc.nist.gov/ refprop/MINIREF/MINIREF.HTM.
22. I.H. Bell, S. Wronski, V. Quoilin. Lemort pure and pseudopure fluid thermophysical property evaluation and the open-source thermophysical property library coolprop. *Ind. Eng. Chem. Res.* **53**, 2498 (2014).
23. *Refprop Database, NIST*; https://www.nist.gov/programs-projects/reference-fluidthermodynamic-and-transport-properties-database-refprop.
24. *ThermodataEngine Database, NIST*; https://trc.nist.gov/ tde.html.
25. *WTT Database, NIST*; https://wtt-pro.nist.gov/wtt-pro/.
26. *MOL-Instincts Database, ChemEssen*; https://www.molinstincts.com/.
27. *ChemRTP Database, ChemEssen*; http:// www.chemrtp.com/.
28. *Phase Diagrams: Understanding the Basics*. Edited by F.C. Campbell (ASM International, 2012).
29. B. Cantor. *The Equations of Materials* (Oxford University Press, 2020).
30. M.A. Anisimov. *Critical Phenomena in Liquids and Liquid Crystals* (CRC Press, 1991).
31. A. Oleinikova, L. Bulavin, V. Pipich. The viscosity anomaly near the lower critical consolute point. *Int. J. Thermophys.* **20**, 889 (1999).
32. JANAF Thermochemical Tables. *J. Phys. Chem. Ref. Data* **11**, 695 (1982).
33. LV. Gurvich, I.V. Veits, C.B. Alcock. *Thermodynamics Properties of Individual Substances*. 4th edition (RAS, 1989) [ISBN: 0-8493-9926-2].
34. W. Wagner, T. Riethmann, R. Feistel, A.H. Harvey. New equations for the sublimation pressure and melting pressure of H_2O Ice Ih. *J. Phys. Chem. Ref. Data* **40**, 043103, (2011).
35. S. Herrig, M. Thol, A.H. Harvey, E.W. Lemmon. A reference equation of state for heavy water. *J. Phys. Chem. Ref. Data* **47**, 043102 (2018).
36. F.A. Deeney, J.P. O'Leary. Zero point energy and the origin of the density maximum in water. *Phys. Lett. A* **372**, 1551 (2007).
37. G. Boato, G. Casanova. A self-consistent set of molecular parameters for neon, argon, krypton and xenon. *Physica* **27**, 571 (1961).
38. D. Santamaria-Perez, G.D. Mukherjee, B. Schwager, R. Boehler. High-pressure melting curve of helium and neon: Deviations from corresponding states theory. *Phys. Rev. B* **81**, 214101 (2010).
39. W.E. Keller. *Helium-3 and Helium-4* (Springer Science + Business Media, 1969).
40. *The McGraw-Hill Dictionary of Scientific and Technical Terms*. 7th edition (McGraw-Hill, 2016).
41. J. Wisniak. Historical development of the vapor pressure equation from Dalton to Antoine. *J. Phase Equil.* **22**, 622 (2001).
42. A.M.A. Dias, J.C. Pamies, L.F. Vega, J.A.P. Coutinho, I.M. Marrucho. Modelling the solubility of gases in saturated and substituted perfluoroalkanes. *Polish J. Chem.* **80**, 143 (2006).
43. N. Matsunaga, A. Nagashima. Prediction of the critical constants and the saturation vapor pressure of tritium oxide. *Ind. Eng. Chem. Fund.* **25**, 115 (1986).
44. H.W. Xiang. Vapor pressure and critical point of tritium oxide. *J. Phys. Chem. Ref. Data* **32,** 1707 (2003).
45. N.H. Fletcher. *The Chemical Physics of Ice* (Cambridge University Press, 1970).
46. P.W. Bridgman. Water, in the liquid and five solid forms, under pressure. *Proc. Am. Acad. Arts Sci.* **47**, 439 (1912).
47. W. Wagner, A. Pruss. The IAPWS formulation 1995 for the thermodynamic properties of ordinary water substance for general and scientific use. *J. Phys. Chem. Ref. Data* **31**, 387 (2002).
48. G.S. Kell. Effect of isotopic composition, temperature, pressure, and dissolved gases on the density of liquid water. *J. Phys. Chem. Ref. Data* **6**, 1109 (1977).
49. J. Horita, D.R. Cole. Stable isotope partitioning in aqueous and hydrothermal systems to elevated temperatures. In: *Aqueous Systems at Elevated Temperatures and Pressures: Physical Chemistry in Water, Steam and Hydrothermal Solutions*. Edited by D.A. Palmer, R. Fernández-Prini, A.H. Harvey (Elsevier, 2004).
50. D.R. White, W.L. Tew. Improved estimates of the isotopic correction constants for the triple point of water. *Int. J. Thermophys.* **31**, 1644 (2010).
51. F. Mallamace, C. Corsaro, D. Mallamace, S. Vasi, C. Vasi, H.E. Stanley. Thermodynamic properties of bulk and confined water. *J. Chem. Phys.* **141**, 18C504 (2014).
52. A. Khan, M. Rezwan Khan, M. Ferdouse Khan, F. Khanam. A liquid water model: Explaining the anomalous density variation of liquid D_2O and shifting of density maximum under pressure. *J. Mol. Struct. (Theochem)* **679**, 165 (2004).
53. P. Gallo, K. Amann-Winkel, Ch.A. Angell, M.A. Anisimov, F. Caupin, Ch. Chakravarty, E. Lascaris, T. Loerting, A.Z. Panagiotopoulos, J. Russo, J.A. Sellberg, H.E. Stanley, H. Tanaka, C. Vega, L. Xu, L.G.M. Pettersson. Water: A tale of two liquids. *Chem. Rev.* **116**, 7463 (2016).
54. J. Russo, H. Tanaka. Understanding water's anomalies with locally favoured structures. *Nat. Commun.* **5**, 3556 (2014).
55. A. Nilsson, L.G.M. Pettersson. The structural origin of anomalous properties of liquid water. *Nat. Commun.* **6**, 8998 (2015).

56. R. Shi, H. Tanaka. Direct evidence in the scattering function for the coexistence of two types of local structures in liquid water. *J. Am. Chem. Soc.* **142**, 2868 (2020).
57. A. Kholmanskiy, N. Zaytseva. Physically adequate approximations for abnormal temperature dependences of water characteristics. *J. Mol. Liq.* **275**, 741 (2019).
58. A. Kholmanskiy. Hydrogen bonds and dynamics of liquid water and alcohols, *J. Mol. Liq.* **325**, 115237 (2021).
59. A. Stepanov. Thermodynamics of substances with negative thermal expansion and negative compressibility. *J. Non-Cryst. Solids* **356**, 1168 (2010).
60. O. Khorolskyi, N.P. Malomuzh. pH and H-bonding energy for pure water. *Chem. Phys. Lett.* **828**, 140713 (2023).
61. O. Khorolskyi, A. Kryvoruchko. Non-trivial behavior of the acid-base balance of pure water near the temperature of its dynamic phase transition. *Ukr. J. Phys.* **66**, 972 (2021).
62. A.I. Fisenko, O.V. Khorolskyi, N.P. Malomuzh, A.A. Guslisty. Relationship between the major parameters of warm-blooded organisms' life activity and the properties of aqueous salt solutions. *AIMS Biophysics* **10**, 372 (2023).
63. M.M. Lazarenko, O.M. Alekseev, S.G. Nedilko, A.O. Sobchuk, V.I. Kovalchuk, S.V. Gryn, V.P. Scherbatskyi, S.Yu. Tkachev, D.A. Andrusenko, E.G. Rudnikov, A.V. Brytan, K.S. Yablochkova, E.A. Lysenkov, R.V. Dinzhos, S. Thomas, T.R. Abraham. Impact of the alkali metals ions on the dielectric relaxation and phase transitions in water solutions of the hydroxypropylcellulose. In: *Nanoelectronics, Nanooptics, Nanochemistry and Nanobiotechnology, and Their Applications. NANO 2022* (Springer, 2022).
64. C. Andreani, C. Corsaro, D. Mallamace, G. Romanell, R. Senesi, F. Mallamace. The onset of the tetrabonded structure in liquid water. *Sci. China Phys. Mech. Astron.* **62**, 107008 (2019).
65. A.G. Lyapin, O.V. Stal'gorova, E.L. Gromnitskaya, V.V. Brazhkin. Crossover between the thermodynamic and nonequilibrium scenarios of structural transformations of H_2O Ih ice during compression. *J. Exper. Theor. Phys.* **94**, 283 (2002).
66. G.S. Kell. Precise representation of volume properties of water at one atmosphere. *J. Chem. Eng. Data* **12**, 66 (1967).
67. P.G. Hill, R.D.Ch. MacMillan, V. Lee. A fundamental equation of state for heavy water. *J. Phys. Chem. Ref. Data* **11**, 1 (1982).
68. M. Goldblatt, The density of liquid T_2O. *J. Phys. Chem.* **68**, 147 (1964).
69. F. Franks. *Water. A Matrix of Life. 2nd edition* (Royal Society of Chemistry, 2000).

Received 24.01.23.
Translated from Ukrainian by O.I. Voitenko

Л.А. Булавін, Є.Г. Рудніков, С.О. Самойленко

ФАЗОВІ ДІАГРАМИ ІЗОТОПОЛОГІВ ВОДИ ТА ІНЕРТНИХ РЕЧОВИН

У роботі наведено фазові діаграми, які розраховано за літературними даними для ізотопологів води та інертних речовин. Проведено перевірку принципу відповідних станів при використанні калоричних змінних. Показано, що у приведених координатах температури, тиску та хімічного потенціалу ізотопологи води складають одну групу речовин і мають подібні фазові діаграми. Разом з тим, інертні речовини, починаючи з аргону, в зазначених координатах утворюють іншу групу речовин з подібними фазовими діаграмами. В той самий час, гелій та неон, для яких квантовий параметр де Бура за величиною є значним, мають фазові діаграми, відмінні від діаграм для інших інертних речовин. Спрогнозовано фазові діаграми тритійованої води T_2O та радону Rn.

Ключові слова: ізотопологи води, надважка вода, інертні речовини, радон, хімічний потенціал, фазові діаграми, рівняння Кірхгофа, функції Масьє, потрійна точка.